

# Photorefractive semiconductors and applications

Li-Jen Cheng

Center for Space Microelectronics Technology  
Jet Propulsion Laboratory  
California Institute of Technology  
Pasadena, California 91109

and

Keung L. Luke

Department of Physics and Astronomy  
California State University  
Long Beach, California 90840

## ABSTRACT

**Photorefractive** semiconductors are attractive for information processing, because of fast material response, compatibility with semiconductor lasers, and availability of cross polarization diffraction, for enhancing signal-to-noise ratio. This paper presents recent experimental results on information processing using **photorefractive** GaAs, InP and CdTe, including image processing with semiconductor lasers. The results demonstrate the feasibility of using **photorefractive** compound semiconductors as dynamic holographic interaction media for information-processing applications in low-power, compact configurations.

## 1. INTRODUCTION

Use of **photorefractive** semiconductors provides a promising fast, parallel approach to information processing. Based on the principles of nonlinear optics and holography, it owes its unique capability to the **photorefractive** effect observed in photoconductive electro-optic materials.

Several semi-insulating compound semiconductors have been demonstrated to be **photorefractive**. They include undoped and chromium-doped gallium arsenide (GaAs, GaAs:Cr),<sup>1,2</sup> iron-doped and titanium-doped iridium phosphide (InP:Fe, InP:Ti),<sup>1,3</sup> undoped gallium phosphite (GaP)<sup>4</sup> and vanadium- and titanium-doped cadmium telluride (CdTe:V, CdTe:Ti).<sup>5</sup> These photorefractive semiconductors provide several attractive features for information-processing applications and could lead to a new generation of integrated optical information processors.

The purpose of this paper is to review the progress of this technologically important area, based mainly on the work carried forward at the Jet Propulsion Laboratory.

This paper is divided into eleven sections. Following the introduction, we describe five important photorefractive properties of GaAs in section 2. We then describe two generic wave mixing configurations for image processing and spatial resolution of GaAs four-wave mixing systems in section 3. Phase conjugate interferometer and its applications are covered in section 4. Image correlation with photorefractive GaAs is treated in section 5. A novelty-fihcred optical correlator using photorefractive CdTe is described in section 6. Image processing with photorefractive InP and with semiconductor lasers are covered in section 7 and 8, respectively. Time correlation is discussed in section 9. Image correlation using a new class of thin photorefractive devices is described in section 10. The review is summarized in the concluding section 11,

## 2. PHOTOREFRACTIVE PROPERTIES OF GaAs

Because the demonstration experiments were mainly on information processing using photorefractive GaAs, this section presents the photorefractive properties of GaAs. Some photorefractive properties of InP and CdTe are stated for comparison purpose,

### 2.1. Basic mechanism

The photorefractive effect refers to the phenomenon of the light-induced refractive index change of an electro-optic material, analogous to the light-induced absorption change known as the photochromic effect. However, the physical mechanism is different.

The light-induced refractive index change in a material is based on the spatial modulation of electrical carrier generation by periodic illumination. When two coherent laser beams interfere in the material to form a fringe pattern, the photoexcited carriers generated in the bright regions diffuse or drift to the dark regions in which they are trapped at localized energy levels in the bandgap, leaving behind in the bright regions fixed charges of opposite sign. This periodic charge redistribution creates a periodic local space-charge field pattern, giving rise to a refractive index grating via the linear electro-optic effect with the same spatial period as the fringe pattern, but shifted one quarter of a period in space from it.<sup>6</sup> This grating acts as a volume hologram and can be used for optical information processing and storage. Because of the charge trapping, the photorefractive effect can be observed with light beams of moderate intensities. For example, photorefractive effects in GaAs can be observed with a total beam intensity less than  $1 \text{ mW/cm}^2$ .<sup>7</sup>

In addition to possessing a non-zero electro-optic coefficient, a photorefractive material must have adequate densities of localized energy levels which can act as the donors and the acceptors for supplying and receiving the transferred charges, respectively. For example, the existence of both neutral and ionized states of the EL-2 center in LEC-grown, undoped, semi-insulating GaAs makes this material photorefractive. Typical concentration of the EL-2 centers in LEC-grown, undoped GaAs is about  $1 \times 10^{16} / \text{cm}^3$ , among which about  $1 \times 10^{15} / \text{cm}^3$  are positively charged acceptors.

The energy band gap of the crystal and the position of the level in the bandgap determine respectively the short and long limits of the wavelength range within which the photorefractive effect exists. For example, the band gap of GaAs is about 1.43 eV and

the responsible EL-2 level in LEC-grown, undoped, semi-insulating GaAs is about 0.75 eV below the edge of the conduction band. Thus, the GaAs crystal can have the photorefractive effect in the wavelength range of about 0.8- 1,6  $\mu\text{m}$ . The effect in CdTe exists approximately in the same wavelength range. The short wavelength limit of InP is about 0.85  $\mu\text{m}$ , because of smaller energy bandgap.

Furthermore, the photorefractive material has to be insulating or semi-insulating in order to avoid the Coulomb screening around the charged centers. Typical resistivity of semi-insulating GaAs is in the order of  $5 \times 10^7$ - $2 \times 10^8$  ohm-cm whereas typical resistivity of InP is about  $10^7$  ohm-cm. This difference is due to the fact that the energy bandgap of InP (1.27 eV) is lower than that of GaAs (1.43 eV). Consequently, photorefractive effect of InP requires higher light intensity or at lower temperatures as illustrated experimentally,

## 2.2. Material response times

The photorefractive response time of a material is the time required for writing an index grating in this material. It depends on the beam intensities, grating period, as well as material properties such as carrier mobility, donor concentration, photoionization cross section of the donor, and carrier capture rate of the acceptor. It has been reported that the response time in LEC-grown, undoped GaAs is about 1 ms and 20  $\mu\text{s}$  under a total intensity of 0.1 and 4  $\text{W}/\text{cm}^2$ , respectively. These values are, at least, about two orders of magnitude smaller than those of the oxides under the same intensities. This provides semiconductors with a clear advantage in the image processing speed. The response time of GaAs can be in the picosecond time scale, if intense light pulses are used. For example, under a total intensity of  $5 \times 10^7$   $\text{W}/\text{cm}^2$ , the response time of GaAs was reported to be 43 ps.<sup>9</sup> However, this picosecond-response photorefractive effect uses two-photon absorption, different from that of the conventional photorefractive effect.

The volume holographic grating written in a photorefractive material has a finite lifetime. This lifetime determines the image storage time in the crystal. It is an important parameter for evaluating the image processing capability. For a given material, the read beam intensity and the grating periodicity are two parameters determining the lifetime. Recently, a beam coupling technique using a 1.15- $\mu\text{m}$  He-Ne laser was employed to measure the grating lifetime in GaAs.<sup>10</sup> The largest lifetime measured is about 8  $\mu\text{s}$  under a read beam intensity of 0.7  $\text{mW}/\text{cm}^2$  with the grating periodicity being 0.63  $\mu\text{m}$ . The measured value decreases to milliseconds as the read beam intensity and the grating periodicity increase to about 10  $\text{mW}/\text{cm}^2$  and 4  $\mu\text{m}$ , respectively. In addition, the results suggest that lifetime is sensitive to residual imperfections in the crystal.

## 2.3. Figure of merit

It is known that the figures of merit,  $n^3r/\epsilon$ , of these semiconductors are similar to those of the oxides,<sup>7</sup> where  $n$  is the refraction index,  $r$  is the electro-optic coefficient, and  $\epsilon$  is the relative dielectric constant.  $n^3r/\epsilon$  is for maximum photorefractive sensitivity of the material. The figures of merit of GaAs, GaP, InP, and CdTe are 3.3, 3.7, 4.1, and 16, respectively, whereas those of BSO, SBN, BaTiO<sub>3</sub>, LiNO<sub>3</sub>, and KNbO<sub>3</sub> are 1.8, 4.8, 4.9,

11, and 14, respectively." CdTe has the highest figure of merit among all the materials stated, slightly larger than  $\text{KNbO}_3$ , and is a potentially superior image processing medium in the near infrared range. Among the semiconductors, the figure of merit of CdTe is about four times larger than those of GaAs, GaP, and InP. This is consistent with experimental results. For example, it was observed that vanadium and titanium doped CdTe crystals had larger photorefractive effects than GaAs and InP without an applied electric field.<sup>5</sup>

A detailed discussion of photorefractive sensitivity is available in the literature.<sup>12</sup>

#### 2.4. Material properties

The photorefractive effect is extremely sensitive to the existence of crystal imperfections, because these defects can drastically reduce the net charge separation efficiency. For example, the concentration of the ionized EL-2 center in LEC-grown, undoped GaAs which acts as the acceptor in the photorefractive process can be increased using an inverted thermal treatment, but the photorefractive gain in the sample was poor. This is due to the fact that the treatment creates a new defect which reduces the net charge separation.<sup>13</sup> Although the technology of GaAs crystal growth is the most advanced one among those of all the compound semiconductors available, it is evident that the photorefractive effect of GaAs crystals (available commercially and from research laboratories) varies considerably among suppliers as well as from one ingot to another." The best observed gain coefficients in GaAs without and with an applied DC electric field (with and without moving grating technique) are reasonably close to those of theoretical prediction based on known concentration of the EL-2 center in comparison with those of photorefractive oxides.] This indicates that the state-of-the-art technology of GaAs can produce good photorefractive crystal. However, given a crystal's growth condition, there is no way to know whether or not it is photorefractive crystal, unless photorefractive measurement is done on it. More research is needed to understand the origin of the detrimental effects and to develop a growth condition of optimized crystals for the photorefractive effect. This argument can be applied to InP as well. However, the CdTe material technology is still not mature in comparison with those of GaAs and InP. More material research effects on CdTe are needed.

#### 2.5. Electric field Effects

. It is known that several techniques can be used to enhance photorefractive effects in semiconductors, for example, applications of a high DC electric field without and with moving grating.<sup>14,15</sup> In addition to the enhancement, the application of an electric field also causes two effects, namely, the increase of material response time and the creation of signal fluctuation. The latter is due to moving charge domains created by the high electric field with speed which increases the field strength and light intensity. The increase of material response time will make the use of photorefractive semiconductors for some applications less attractive. Nevertheless, good correlation images with enhancement of 100 in diffraction efficiency were obtained as illustrated by the results to be presented

later. In addition to the conventional photorefractive effect using the linear electro-optic property, the large photorefractive effect based on the Franz-Keldysh effect under a DC electric field with and without moving grating technique was recently observed in GaAs<sup>16</sup> and InP.<sup>17</sup> This enhanced effect has not yet been investigated for image processing applications.

### 3. WAVE MIXING CONFIGURATIONS FOR IMAGE PROCESSING

There are two generic configurations for optical information processing using the photorefractive effect, namely, two-wave mixing (beam coupling) and four-wave mixing. The latter includes degenerate and non-degenerate four-wave mixing configurations with and without polarization switching. A brief discussion on these configurations is given next.

#### 3.1. Two-wave mixing

In the two-wave mixing configurations, two coherent beams intersect in a crystal and create an index grating via the photorefractive effect. In general, the interference pattern of these beams and the induced index grating are 90 degrees out of phase. This leads to an unsymmetrical diffraction of the incident beams by this index grating and results in a net intensity transfer from one beam to another. If the intensity gain of one beam is larger than the absorption in the material, the intensity of this beam is amplified. This effect, initially observed in photorefractive LiNbO<sub>3</sub> crystals,<sup>18</sup> can be used for amplifying the intensity of an information-bearing optical beam as initially demonstrated by Kukhtarev et. al in LiNbO<sub>3</sub>.<sup>19</sup> Two-beam coupling together with the polarization switching property of GaAs crystals can also be used to implement spatial light modulation as recently demonstrated.<sup>20</sup>

#### 3.2. Degenerate four-wave mixing

In the four-wave mixing configurations, two coherent beams write an index grating and a third beam reads the grating, creating a fourth (i.e. output) beam by diffraction. In the degenerate four-wave mixing, the diffracted beam travels against one of the write beams and is phase conjugate to the write beam. The degenerate four-wave mixing configuration is more useful and versatile. A number of basic image processing operations, including phase conjugate imaging, edge-enhancement, correlation<sup>21,22</sup> and convolution, vector-vector multiplication,<sup>23</sup> and interferometry,<sup>24,25</sup> were demonstrated using GaAs in the degenerate four-wave mixing configuration. The crystals can be used in both the reflection and transmission modes, depending on the beam geometry and the crystal orientations. For GaAs, the transmission mode has a faster response time but a smaller diffraction efficiency, whereas the reflection mode has a slower response time but a larger diffraction efficiency. This is because these two modes have different grating spacing ranges and the response time and the diffraction efficiency decrease as the grating spacing becomes larger.

### 3.3. Non-degenerate four-wave mixing

In the non-degenerate four-wave mixing configuration, one can write the information-bearing grating with one wavelength and read it with another. A potential use of non-degenerate four-wave mixing is that if the information-bearing index grating is to be preserved after the readout operation, one can read the grating with a longer wavelength that does not erase the grating. Image transfer from a beam at  $1.06 \mu\text{m}$  to another at  $1.3 \mu\text{m}$  was demonstrated using GaAs.<sup>23</sup>

### 3.4. Polarization switching

Crystal structures of GaAs, InP, CdTe, and GaP are  $\bar{4}3m$  cubic group symmetry. The optical isotropy and tensor nature of the electro-optic coefficients of these crystals permit the possible cross polarization switching in beam coupling and four-wave mixing.<sup>26,28</sup> Such cross polarization switching is possible only along a special direction in BaTiO<sub>3</sub> and SBN because of their optical anisotropy. In BSO, the circular birefringence strongly influences the polarization of the diffracted beam. The polarization switching has been very important for image processing using GaAs because its electro-optic efficiencies are small. Use of polarization switching is an effective way to enhance the signal-to-noise ratio. Most experiments on image processing using GaAs were done with a polarization switching configuration,

Figure 1 gives two four-wave mixing configurations with and without polarization switching effect. The two configurations use the crystal in different orientation with respect to the beam arrangement as indicated in the figure. Two write beams propagate codirectionally. In the configuration with polarization switching, the [001] direction of the crystal is perpendicular to the incident plane of the beams. The polarization directions of the write beams and the read beam are in the incident plane. Because of polarization switching, the diffracted beam is polarized in the direction perpendicular to the incident plane and can be separated easily by a polarizing beamsplitter. This configuration provides excellent signal-to-noise ratio. In the configuration without

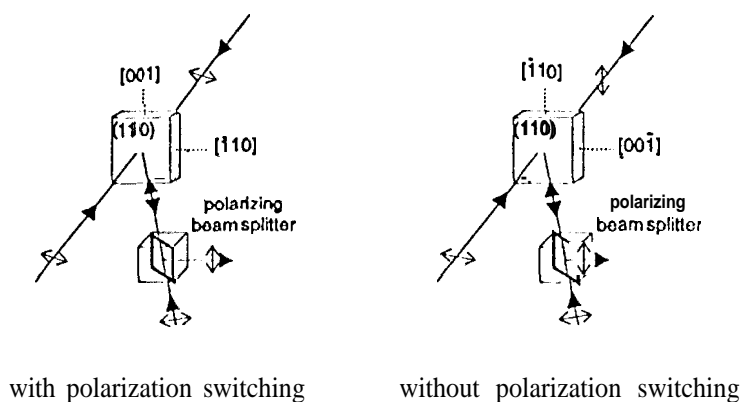


Figure 1, Examples of degenerate four-wave mixing configuration.

polarization switching, the [11 0] direction is perpendicular to the incident plane. The polarization of the read beam has to be perpendicular to the incident plane in accordance with the electro-optic tensor properties. In this configuration, some scattered light from the read beam can mix with the diffracted beam. Therefore, the signal-to-noise ratio is lower.

### 3.5. Spatial resolution of GaAs four-wave mixing systems

Four-wave mixing systems can resolve an image with a spatial resolution limited by the index grating periodicity which is a function of the wavelength and the incident angles. It has been demonstrated that degenerate four-wave mixing in a ruby crystal can produce phase conjugate images with a resolution better than 500 lp/mm using 0.514- $\mu$ m laser light?

To investigate the spatial resolution of photorefractive GaAs image processing systems, a vector-vector outer product experiment and a phase conjugation experiment were performed using Ronchi gratings as the input patterns. Figure 2 shows a schematic of the experimental setup used.<sup>25</sup> Experimental results show that this setup could resolve the rectangular dot array clearly when a pair of 20 lp/mm Ronchi gratings were used, but not with a pair of 100 lp/mm Ronchi gratings. However, if the Ronchi grating in the pump beam 1 was removed, the line array picture of another Ronchi grating (namely the phase conjugate image of the input pattern in the probe beam) could be clearly seen. When a 250 lp/mm Ronchi grating is placed in the probe beam, the phase-conjugation setup also failed to resolve it.

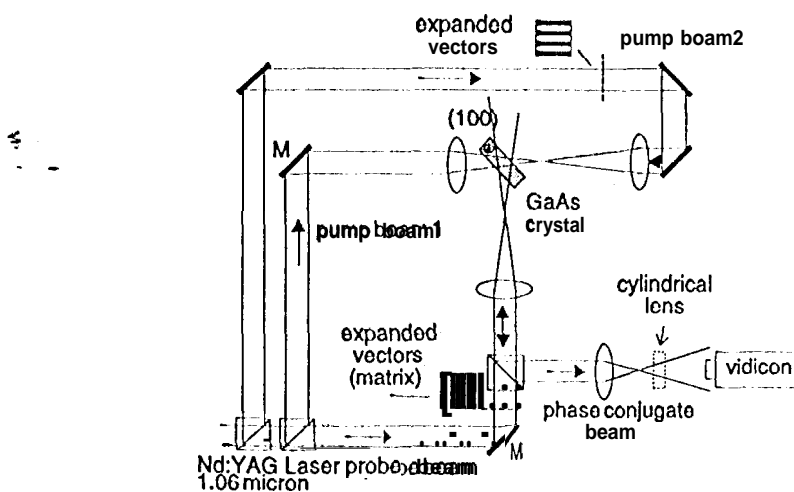


Figure 2. Schematic of experimental set-up used to investigate spatial resolution,

## 4. PHASE CONJUGATE INTERFEROMETER AND ITS APPLICATIONS

### 4.1. General

It is well-known that photorefractive crystals are volume holographic media. Because of the nature of volume holograms, in principle, it is possible to read and write multiple volume holograms with slightly different orientations superimposed in the same photorefractive crystal without causing notable cross talk. Figure 3 shows the schematic diagram and results of a multiple hologram writing and reading experiment. The "common" write beam generates a "hologram with each of the image-bearing write beams. Each hologram carries a different spatial information and is superimposed on another in the crystal. The read beam is diffracted by each hologram separately. The output beams are then coupled out by a beam splitter and captured by a CCD camera. This experiment has established a base on which a phase conjugate interferometer can be built,

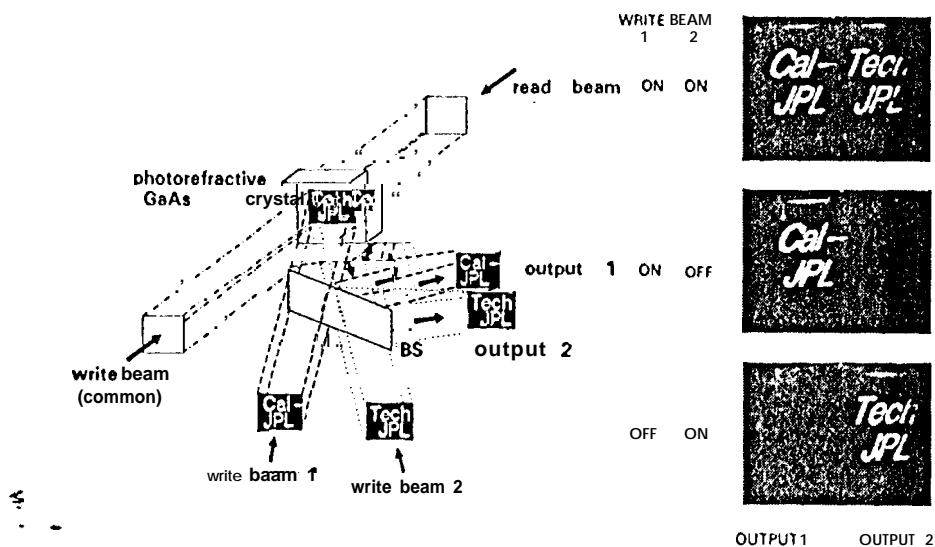


Figure 3. Schematic of a multiple degenerate four-wave mixing configuration with overlapping grains (left). Photographs (right) illustrate the experimental results.

### 4.2. Phase-conjugate interferometer

Coherent image subtraction and addition can be achieved with an interferometer, such as the Michelson interferometer. In practice, the image intensity drifts between the extremes because of the phase fluctuation due to ambient air currents and/or thermal drift and also is extremely sensitive to misalignment. The use of fast photorefractive phase conjugate mirrors which replace the ordinary mirrors can overcome both problems, as demonstrated by experimental observations.

The use of an interferometric configuration with a phase conjugate mirror of BaTiO<sub>3</sub><sup>36,34</sup> and BSO<sup>35</sup> for parallel image operations was previously reported. Because of the nature of phase conjugate mirrors, these phase conjugate interferometers are more stable in operation and easier to align than those using conventional mirrors only. However, operations with these materials are slow and sensitive to environmental fluctuations, such as air turbulence and low-frequency vibrations of optical components.

The fast response of compound semiconductors, such as GaAs, not only provides high speed operation of a phase conjugate interferometer, but also makes the system immune to low-frequency vibration of optical components. The latter is due to the fact that the light-induced grating can follow the slow motion induced by low-frequency vibration.

#### 4.3. Applications

Several basic computing operations using a GaAs phase conjugate interferometer have been demonstrated. These include image subtraction, coherent and incoherent image addition, image inversion, OR and exclusive OR (XOR) logic operations.<sup>25</sup>

Time variation of spatial information can be detected using a phase conjugate interferometer. This property is important for motion detection, novelty filtering and target tracking, which were demonstrated using BaTiO<sub>3</sub> by Anderson and coworkers.<sup>36,37</sup> Fast semiconductors can be used to make high-resolution fast novelty filters to track a target in a more precise way.<sup>3</sup>

### 5. IMAGE CORRELATION USING PHOTOREFRACTIVE GaAs

#### 5.1. General

Optical Image correlation takes full advantages of light, namely, parallel operation and global interconnection in implementing Fourier transforms by a lens. Photorefractive compound semiconductors can provide this type of high-speed implementation.<sup>21,22</sup>

According to the correlation theorem, the correlation contains Fourier transforms of input and reference images, multiplication of transformed images in the Fourier domain, and inverse Fourier transform of the product.<sup>39</sup> This process can be implemented using two lenses and a photorefractive crystal to provide Fourier transform and multiplication, respectively. In addition, the photorefractive crystal also serves as a temporal recording medium.<sup>40,41</sup> There are two configurations of implementation, namely, matched filter<sup>49</sup> and joint transform.<sup>39</sup> In the matched filter method, the hologram of the Fourier transformed incoming scene is recorded in the crystal, whereas, in the joint transform method, the hologram of the product of the two transformed images is written. The matched-filter method is the preferred one, because it does not require re-writing of the hologram whenever any reference image is changed.

It is worthwhile to note that the space bandwidth product of the thick volume hologram will limit the spatial resolution of the photorefractive-crystal-based image correlator.<sup>25</sup> Presumably, the spatial resolution of the GaAs image correlator could be of the same order of magnitude of 20 lp/mm, because the same lenses were used for both

experiments. Obviously, more detailed experiments are needed to determine the accurate values.

In the GaAs photorefractive correlator used in this investigation, the incoming scene is stored in the crystal as a hologram in the Fourier domain and then the template matching process occurs at the diffraction of the reference object-bearing read beam at the hologram as illustrated in the upper part of Fig. 4. This configuration provides two distinctive advantages: (1) incoming scene can have a large incident angle, and (2) an extremely fast template matching process.

When the time needed for writing a hologram is about equal to or shorter than the time of inputting the scene, the correlator can track targets in real time. Because of fast material response, the photorefractive semiconductor correlator is suitable for real-time tracking applications. Slow photorefractive crystals, such as BaTiO<sub>3</sub>, cannot provide real-time target tracking, because the grating formation in the crystal is too slow to follow the change of the incoming scene.

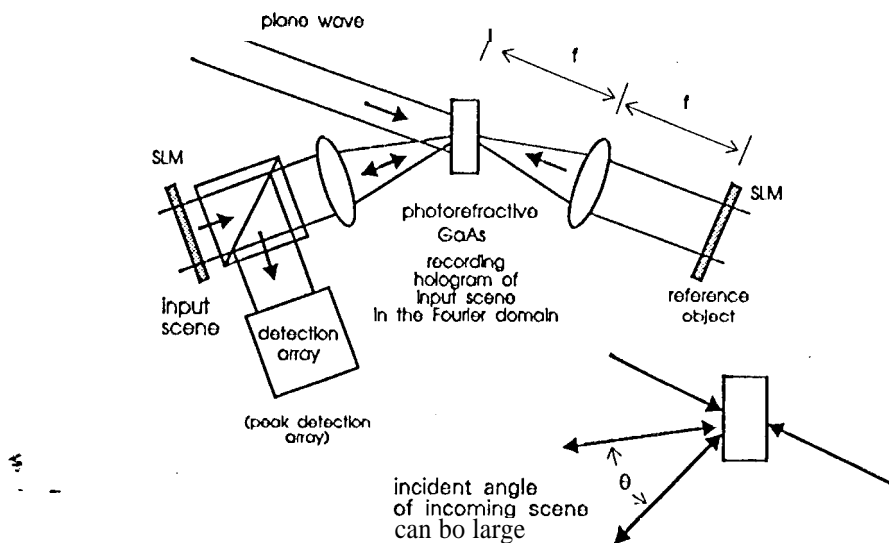
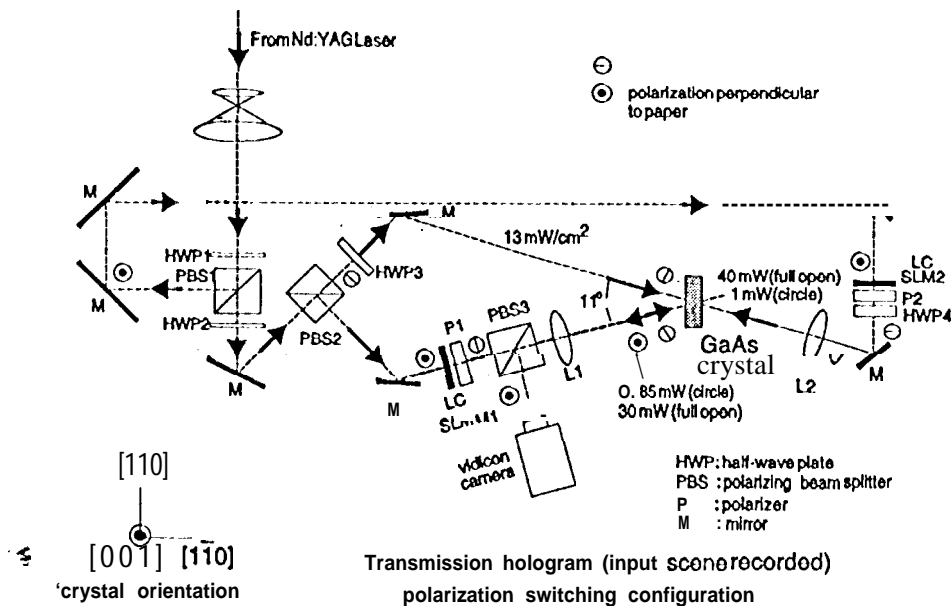


Figure 4. Matched-filter image correlation configuration using degenerate four-wave mixing in photorefractive GaAs which records a hologram of the input scene in the Fourier domain; the template-matching process occurs at the diffraction of the reference object-bearing read beam at the hologram (upper figure). The time required for the template-matching process is the travel time of the light beam from the reference object input device through the diffraction in the crystal to the detector array, typically in the time scale of nanoseconds. The incoming scene can have a large incident angle because of the nature of degenerate four-wave mixing, as illustrated by the schematic at the lower right.

## 5.2, Experiment

In our "previous work,"<sup>21</sup> input images were put on photographic films. Recently, experimental data on an optical image correlator using a photorefractive GaAs crystal and two modified liquid crystal television (LCTV) screens as spatial light modulation input devices were reported.<sup>22</sup> The LCTV screens are from a low-cost commercial home grade projection TV (EPSON Crystal Image Video projector). Because of the high contrast ratio (100: 1) of these LCTVs, the quality of some output images of the current correlator is very close to those obtained with transparencies. The frame rate of this correlator is limited by the speed of the LCTVs and vidicon camera used, which is about 30 frames/s. Figure 5 shows a sketch of the experimental setup which is in a matched-filter configuration.



**Figure 5.** Schematic of the experimental set-up using degenerate four-wave mixing in photorefractive GaAs with two electrically addressed liquid crystal spatial light modulators modified from an EPSON liquid crystal television projector. The experiment used polarization switching to minimize stray light,

### 5.3. Experimental observations

#### 5.3.1. High-quality correlation

Two pictures on the left side of Fig. 6 give autocorrelation images of a gray-scale car and an edge-enhanced image of the same car (produced with by a digital computer) and signal profiles taken along the path indicated by solid lines. The autocorrelation signals

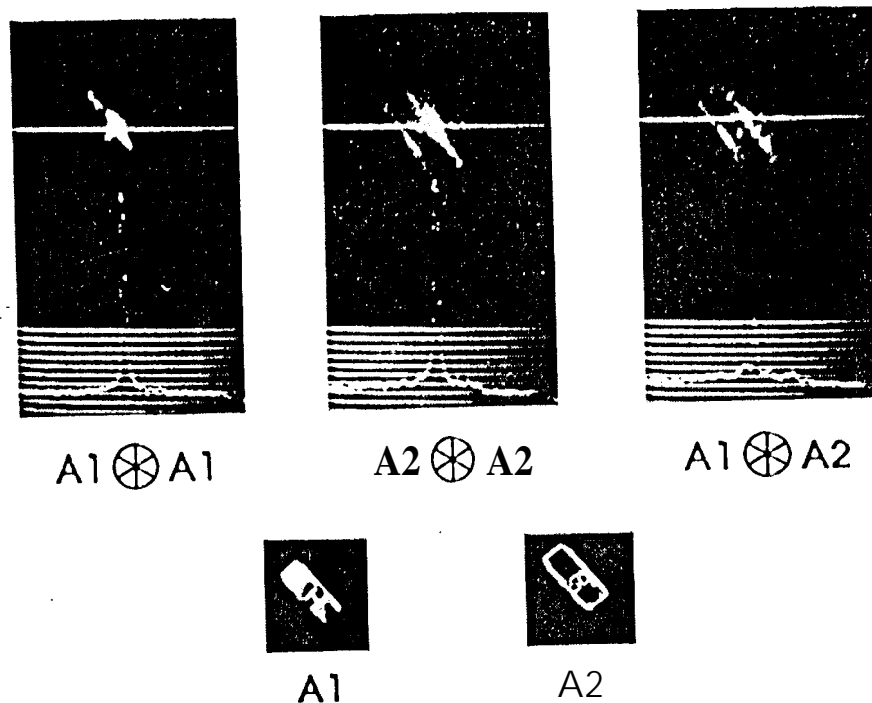


Figure 6. Autocorrelation images of a grey-scale car and an edge-enhanced image of the same car by a digital computer, illustrating that the photorefractive correlator can perform edge enhancement automatically. However, the amplitude of the crosscorrelation peak of the grey-scale car and the edge-enhanced image is only one-third of that obtained from the autocorrelation, indicating that the result from optical edge enhancement is slightly different from that made by a digital computer.

are strong and sharp as shown in the pictures. This is expected from a true matched-filter implementation,

### 5.3.2. Automatic edge enhancement

A comparison of the scan signals in the two pictures reveals that the two correlation peaks have the same size, which is consistent with the demonstrated fact that edge-enhancement process does occur in the photorefractive process because of the saturation of the DC component of the hologram in the Fourier domain. However, the signal of the cross correlation between the gray-scale car and the edge-enhanced car is much smaller as indicated in the picture at the right. This is due to the fact that the edge-enhanced image of the car generated with a digital computer is slightly different from that by the photorefractive process, demonstrated in a separate experiment. The results illustrate that the edge-enhancement is an inherent phenomenon in the correlation operation using a photorefractive material.

### 5.3.3. Submillisecond response time

Because the frame rate of the LCTV spatial light modulators is about 30 Hz and the material response time is much shorter than  $1/30$ s, it is necessary to insert a fast chopper device in the path of the probe beam for switching light on and off to measure the response time of the GaAs crystal which is an important parameter limiting the input speed of incoming scene for future GaAs correlator. The signal of the GaAs correlator was measured by a Ge detector with the probe beam being chopped. The rise time of the correlation signal was measured as a function of the total laser intensity for a beam ratio of read beam : probe beam : reference beam = 100:70: 1 (measured before the beams transmitted through LCTVs). Since the maximum transmission of the LCTVs used is about 80%, the total intensity used for the correlation process in the photorefractive crystal is only about 8% of the total laser intensity or less. The measured response time of the correlator is inversely proportional to the light intensity, which basically agrees with the photorefractive theory. The shortest response time, measured was 0.8 ms at a total laser intensity of about  $1.5 \text{ W/cm}^2$  and a grating spacing of about  $6 \mu\text{m}$  (angle between write beams =  $11^\circ$ ). In our experiment, about 92% of the total laser intensity is wasted because of the poor transmission of the LCTV. If the transmission can be improved, the correlator can either operate at a much faster rate for the same laser power or at a fixed rate with a much reduced laser power, or a combination. The experimental data obtained so far have demonstrated that the GaAs correlator can operate at a rate of at least 1000 frames/s. Based on the known material response time, the speed of the GaAs correlator can be in the order of several tens of thousand frames/s when the intensity increases.

### 5.3.4. Enhancement of correlation signal by DC electric field

Application of a DC voltage can substantially enhance photorefractive effects. An experiment was performed to examine the effect of a DC electric field on the signal from the GaAs correlator. The data reveal that a 4-kV voltage can enhance the correlation signal by a factor of about 100 and also increase the response time by a factor of 20.<sup>50</sup> There is a tradeoff for the system operation when an enhancement of the signal by an applied voltage is desired.

### 5.3.5. Noise effects

The capability of recognizing objects in a cluttered environment is a very important parameter for evaluation of a potential correlation system. An experiment was carried out with the objective to examine the effect of random dot noise added to the input scene. The noise density, defined as the percentage of the total area covered by the random dot noise, increases from 10% to 60%. The correlation peak with 10% is found to be the same as that without noise, showing that noise of 10% or less has no effect on the correlation. However, 20% noise reduces 40% of the peak, when 60% of the area covered by the noise, the peak is reduced to about one twelfth of the original size, but the peak is still observable. The peak is not observable with the noise occupying 70% of the area. The present result reveals clearly that the GaAs correlator can perform well when the noise is

less than 60%.<sup>50</sup> The mechanism of the peak reduction due to the noise is not clear at this moment. Further investigation is needed in this important area.

### 5.3.6. Other characteristics of GaAs correlators

#### Capability of tracking objects

Because of fast response, the correlation using photorefractive GaAs is capable of tracking objects, as demonstrated experimentally. It is noted that this is not possible if a photorefractive material with a slow response, such as BaTiO<sub>3</sub>, is used,

#### No need for preprocessing Fourier transform of reference objects

The photorefractive correlation system uses optical lenses for Fourier transform. Therefore, there is no need for any preprocessing Fourier transform of reference objects and the system is suitable for applications where real-time selection of reference objects are needed,

#### Easy alignment

It is worthwhile to mention that the correlation process using photorefractive effect requires only the three light beams intersecting in the crystal. There is no need for alignment in pixel accuracy as required by some correlation architectures, such as a binary phase-only filter correlator.

## 6. NOVELTY-FILTERED OPTICAL CORRELATOR

Recently, several authors<sup>21,40-48</sup> have demonstrated real-time optical correlator using photorefractive crystals. In Ref.,48, a video frame rate operation was achieved using a photorefractive GaAs crystal and two Liquid Crystal TV (LCTV) based spatial light modulators. This optical correlator could potentially operate at a frame rate of > 1000 frames/s, provided other parts of the system have comparable speeds. Furthermore, because both the input and reference images are automatically edge enhanced in the correlator, the profile of the autocorrelation peak is sharper and most background caused by the clutters are reduced.

In a follow up work to Ref. 48, we discovered that under a different condition described later, the output peak intensity of a matched object may be increased more than two to three times by simply moving that object.<sup>51</sup> This may be potentially useful to those applications in which only the moving object of interest is desired to be identified and tracked. However, we also observe that the output peak intensities of other matched objects that are not moving also go up by approximately the same amount. This last feature could be either an advantage or disadvantage, depending on the applications.

We call this new optical correlator a novelty-filtered optical correlator (NFOC), because functionally it is similar to the combination of an optical novelty filter<sup>52</sup> and an optical correlator. The basic configuration is a VanderLugt<sup>49</sup> correlator consisting of a

photorefractive crystal which does both the correlation and novelty filtering. The operation principle is thus very different from actually combining an optical novelty filter with an optical correlator.

A schematic and photograph of a novelty-filtered optical correlator are shown in Fig. 7 and Fig. 8, respectively. The basic configuration is the same as a VanderLugt correlator with a *reflection* grating.

Figure 9 shows a pair of the photographs with the target at rest and in motion, illustrating that the correlation peak intensity of the target in motion is about twice of that at rest. This is an observation of correlation enhancement due to target motion.

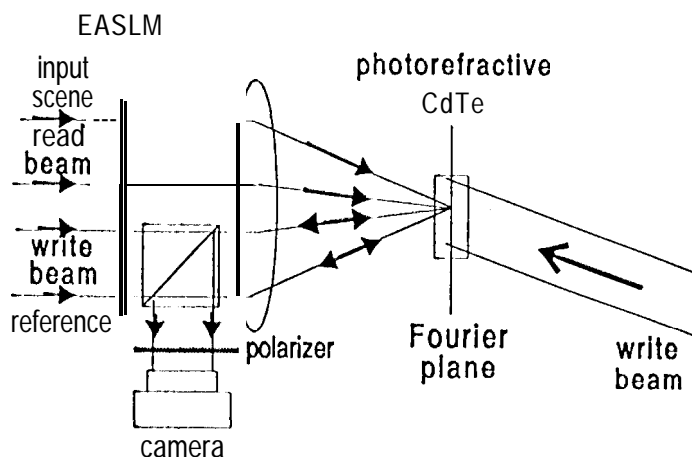


Figure 7. Schematic of a novelty-filtered optical correlator.

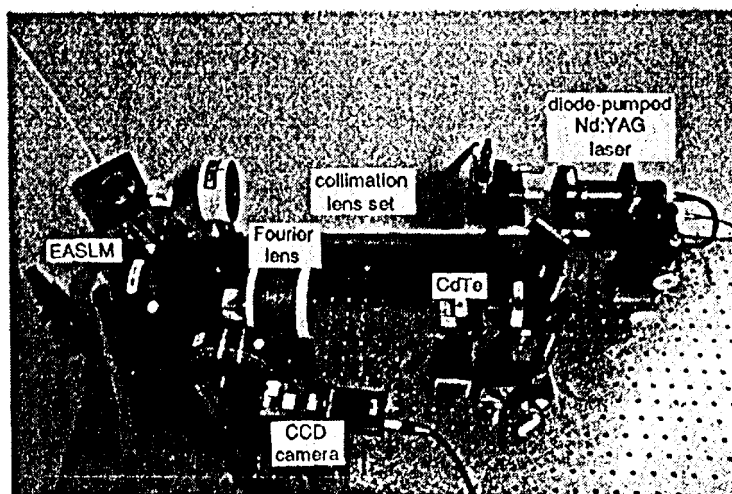


Figure 8. Photograph of a novelty-filtered optical correlator.

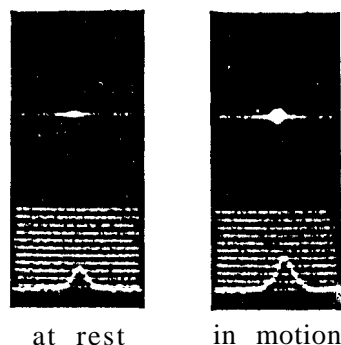


Figure 9. Correlation signal with object moving is about two times stronger than that when object is at rest.

In Ref. 51 a simple qualitative explanation based on the correlation beam geometry in the photorefractive crystal is given to show how the motion enhancement in correlation signal can occur.

#### 7. IMAGE PROCESSING USING PHOTOREFRACTIVE InP

The observation of photorefractive effects in InP and GaAs was simultaneously reported in 1984, \* Photorefractive Fe-doped InP provides potential advantages in comparison with GaAs, namely, figure of merit for photorefractive effect of InP is about 4.1, whereas that for GaAs is about 3.3. In this section, results from a study on the feasibility of using photorefractive InP for optical image processing are reported.

A polished liquid-encapsulated Czochralski-grown Fe-doped InP crystal was used in the study. This sample did not have anti-reflection coatings because of peeling off anti-reflective aluminum oxide layers from InP. The sample dimensions are 5mm x 6mm x 7mm. The experiment includes imaging by phase conjugation and image edge enhancement. The experimental setup was similar to those used for the GaAs experiment'. Images obtained by the phase conjugation process and edge enhancement has good quality,<sup>50</sup> even though the measured diffraction efficiency in the InP sample was about a factor 10 smaller than those of the GaAs samples obtained previously and the beam intensities needed were considerably higher, A possible reason for the low diffraction efficiency and high intensity requirement in the InP sample could be due to that the energy bandgap of InP (1.27eV) is lower than that of GaAs (1.43eV). Consequently, the InP has a high dark conductivity which reduces the photorefractive effect,

in order to verify this explanation, an experiment to measure the two-beam coupling coefficient as a function of beam intensity and temperature was carried out. Results taken at 0, 6, and 19°C under a total beam intensities from 8 to 700 mW/cm<sup>2</sup>, show that the beam coupling coefficient of the InP sample increases with decrease of the temperature and increase of the intensity.~” The same phenomenon in GaAs was observed previously, but occurs at higher temperatures” (60- 100°).<sup>7</sup> The photorefractive effect in the InP

sample at 19°C was not saturated when the total intensity was about 700 mW/cm<sup>2</sup>, whereas the effect in GaAs at the same temperature was saturated when the total intensity was only about 100 mW/cm<sup>2</sup>.<sup>7</sup> These observations are consistent with the thought that image processing in InP requires higher beam intensities at room temperature in order to use full potential of the material because of the high dark conductivity due to the smaller bandgap.

## 8. IMAGE PROCESSING USING SEMICONDUCTOR LASERS

Image processing in **photorefractive** semiconductors with semiconductor lasers is a critical experiment to demonstrate the feasibility of integrating the **photorefractive** processor and the semiconductor laser to develop a functional compact processing module. JPL has successfully performed two proof-of-the-concept experiments on image processing in a **photorefractive** GaAs crystal with two 1.3- $\mu$ m, 13-m W, DFB single mode **GaInAsP/InP** lasers supplied by Ortec Corporation. One experiment was imaging by phase conjugation. The other is image correlation. The results demonstrated the feasibility of integrating **photorefractive** semiconductors and semiconductor lasers together to develop compact image processors.

### 8.1. **Imaging** by phase conjugation

One laser provided two coherent beams to form a hologram in the crystal and the beam from the other laser read the information in the **hologram**.<sup>9</sup> This architecture is **necessary**, because (1) the combination provides a higher total beam power for the four-wave mixing, and (2) the incoherence between the read beam and the write beams eliminates the mode competition that occurs when all three beams originate from a single-mode laser because of its extremely long coherent length.

A reasonably good phase conjugate image was obtained from the experiment. To our knowledge, this is the first observation of phase conjugation imaging in a four-wave **mixing** using a **photorefractive** semiconductor with semiconductor lasers. The result **demonstrates** the feasibility of integrating the **photorefractive** processor and the semiconductor laser to develop a functional compact processing module.

Time scans of the phase conjugate signal were taken with the forward pump beam chopped or the read beam chopped. Results show that (1) the grating formation was about 10 ms, which reveals that the optical process can operate at a speed better than the video frame rate, and (2) the read beam can create enough **photoexcitation** for reducing the grating strength in the crystal and consequently the diffraction by about 60%. The time constant of this process was about 5 ms.<sup>50</sup>

### 8.2. Image correlation

We have demonstrated, for the first time, image correlation using the four-wave mixing in **photorefractive** GaAs with two 1.3- $\mu$ m single-mode, DFB **InGaAsP/InP** lasers. The result provides further support to the statement in the previous subsection that the

feasibility of developing compact integrated optical processing modules with photorefractive and lasing phenomena in compound semiconductors.

Figure 10 shows a schematic of the experimental setup for the image correlation experiment. As indicated in the figure, wavelengths of the two lasers are slightly different, about  $0.0104 \mu\text{m}$ . This difference makes the four-wave mixing configuration non-degenerate.

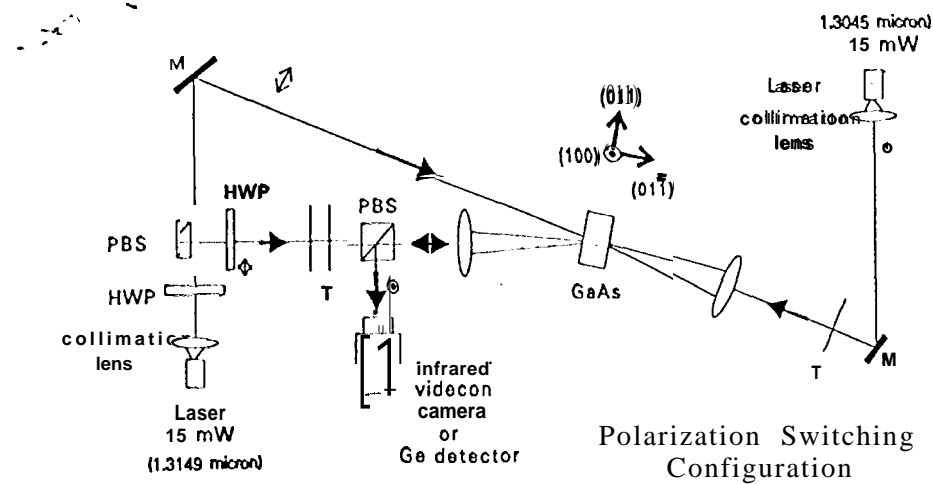


Figure 10. Schematic of the experimental set-up for the image correlation experiment.

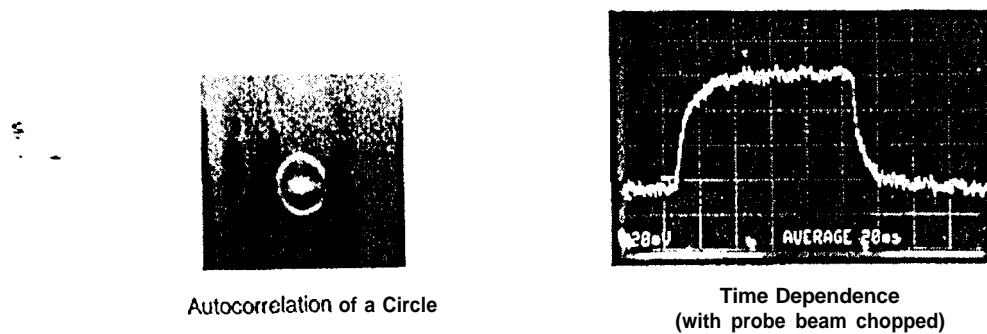


Figure 11. (a) An autocorrelation image of a circle obtained from an experiment using semiconductor lasers. (b) Autocorrelation signal with the probe beam chopped, showing a S-ins characteristic time for hologram formation in the correlation configuration.

Figure 11(a) gives an autocorrelation image of a circle obtained from the experiment. The correlation signal is reasonably good, but its intensity is weak in comparison with those obtained from the experiments using  $1.06\text{-}\mu\text{m}$  beam of similar intensities from a

Nd:YAG laser. This can be attributed to fact that the absorption coefficient of the EL-2 level is about a factor of eight smaller than that at 1.06  $\mu\text{m}$ ." If single-mode semiconductor lasers can provide beams of wavelength around 1  $\mu\text{m}$  with power in several tens of mW are available, a compact image correlator with semiconductors can be developed.

Figure n(b) gives an oscilloscope picture obtained with the probe beam chopped, showing the characteristic times of the hologram formation in the correlation configuration, the formation time and the decay time of the hologram are roughly the same, about 5 ns, illustrating that this correlation system can process input signal at 200 frames/s.

## 9. TIME CORRELATION

Time-integrating correlator has been implemented using acousto-optic (AO) devices and a linear charge-couple-device (CCD) detector arrays.<sup>53,54</sup> The drawback of using a CCD array is that it detects only the correlation term but extraneous bias terms as well. Recently it has been demonstrated that this problem can be removed by replacing the CCD array with a photorefractive crystal.<sup>55,56</sup>

A potential application of the photorefractive time-integrating correlator is in a real-time radar-jamming-interference rejection system using the adaptive filter method. The response time of the photorefractive crystal determines both the integration time and maximum repetition rate of the time integrator, and thus a fast photorefractive crystal such as GaAs can be beneficial in this application.

A GaAs-based photorefractive time-integrating correlator with the same configuration as that described in Ref. 56 was used to perform the crosscorrelation of signals  $S_1$  and  $S_2$  represented by the following equation,<sup>57</sup>

$$S_{12}(\tau) = C \int_0^t S_1(t - x/v) S_2(t + x/v) dx \quad (1)$$

It

carries out this mathematical operation this way. Radio frequency (RF) signals  $S_1(t)$  and  $S_2(t)$  are applied to excite two acoustic waves propagating along AO devices AO 1 and AO2 in opposite directions. Two coherent beams, diffracted by these acoustic waves, are then transmitted through appropriate optics to image and superimpose the patterns of these acoustic waves onto a photorefractive crystal. The resultant refractive index is then read out by the reading beam, yielding a readout beam whose amplitude is spatially modulated according to the correlation function,  $S_{12}(\tau)$ . The output at a square-law detector array is then proportional to  $|S_{12}(\tau)|^2$ .<sup>57</sup> For a detailed review of this topic, see the article by Hong on the applications of photorefractors for signal processing in this volume.

The response time of the GaAs crystal in the time-integrating correlator was measured as a function of the total beam intensity. At a total writing beam intensity of 4  $\text{W}/\text{cm}^2$ , we obtained a response time of better than 80 ns. The dynamic ranges of both the AO device and GaAs crystal in the correlator were also measured and both are about

equal to 40 dB. The response time and dynamic range can probably be improved by using higher laser intensity and better detector,

Because of the vertical alignment of the Bragg cells in the configuration used in our experiment, we observed an interesting new phenomenon - an interference fringe pattern (see Fig. 12) - in the output of the system under certain conditions.<sup>5</sup> A theoretical explanation in good agreement with experimental data is presented below.

Let us consider the case in which the RF input signal to the Bragg cells are square-wave modulated FM signal, namely, the signal contains two different RF frequencies-appearing alternately with time. When the high frequency,  $f_m$ , is applied to the Bragg cells, the diffraction angle is larger than that of the diffracted beam when the lower frequency,  $f_n$ , is applied. The two sets of write beams are in two different planes intersecting at an angle (see Fig. 12). As a result, the index gratings in the photorefractive crystal also intersect with the same angle. The two index gratings may coexist in the crystal if the RF frequency switches between  $f_n$  and  $f_m$  at a rate faster than the reciprocal of the response time,  $\tau_r$ , of the photorefractive crystal. Under this condition, the two index gratings may interfere with each other and result in a fringe pattern as shown in the thicker solid lines in Fig. 12. The maxima of the fringe occur at where the two index gratings are in phase, while the minima occur at where the two index gratings are out of phase.

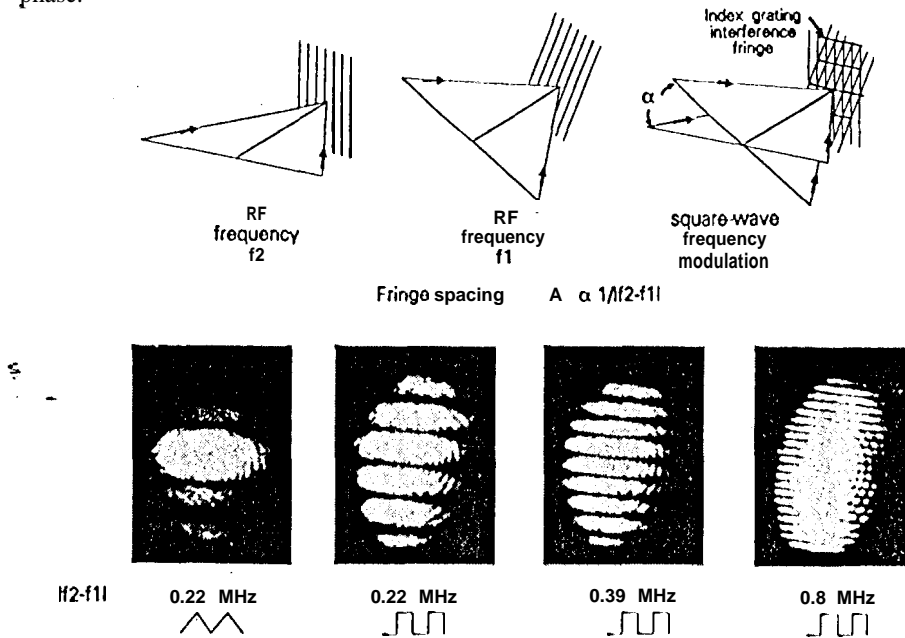


Figure 12. Top: Illustration of the formation of the fringes created by the interference between the index gratings generated by two different RF frequencies. Note that the write beam planes corresponding to frequency 1 and frequency 2 intersect at an angle  $\alpha$ . As a result, the index gratings corresponding to these two sets of write beams also intersect with the same angle. The maxima of the fringes occur at where the two index gratings are in phase, while the minima occur at where the two index gratings are out of phase. Bottom: Images of the index grating interference fringe patterns. The measured spacing between fringes are consistent with the prediction of Eq. (2).

The fringe spacing,  $\Lambda_f$ , can be derived from the beam geometry which is a function of the RF frequency, the sound velocity  $v$  in the AO crystal, and the focal lengths of the lenses. In practice, it is reasonable to assume the diffraction angle of the grating in the Bragg cells is very small. Under this assumption,

$$\Lambda_f = (v/2\Delta f_r) (f_1/f_2) \quad (2)$$

where  $\Delta f_r = f_{r2} - f_{r1}$ ,  $f_1$  is the focal lengths of lenses  $L_1$  and  $L_2$ , and  $f_2$  is the focal lengths of lenses  $L_3$  and  $L_4$ .

- 'Equation (2) is in good agreement with experimental data. For example, the fringe spacing is proportional to  $f_r$  as shown in Fig. 12. For  $f_1 = f_2$ ,  $v = 616$  m/s, and  $\Delta f_r = 0.8$  MHz, both the experimental measurement and the calculation given by Eq. (2) yield  $\Lambda_f = 0.4$  mm. The experimental data also show that  $\Lambda_f$  is inversely proportional to  $f_r$  and independent of the response time of the photorefractive crystal as predicted by Eq. (2).

The observation of the index grating interference fringe in a photorefractive crystal in a time-integration and correlation system is very important to its operation. For chirped signals, the intercepting angle of two write beams is continuously changing. As a result, the strength of the hologram may not increase linearly with time. Under certain special conditions, the strength could be reduced.

#### 10. IMAGE CORRELATION USING A NEW CLASS OF THIN PHOTOREFRACTIVE DEVICES

Recently an optical image correlator using a 2- $\mu$ m-thick GaAs/AlGaAs semi-insulating multiple quantum wells (SI-MQW) and diode lasers was successfully demonstrated." The thinness of this type of device could potentially alleviate the space-bandwidth product (the number of resolvable dots discussed in sec. 3.5) limitation of optical correlator systems based on thick (1-5 mm) photorefractive crystals. Although the resolution of the SI-MQW device used in the experiment is  $\sim 30$   $\mu$ m, the theoretical limit of this class of devices is  $\sim 2.5$  pm. The MQW was doped with  $10^{16}$ /cm<sup>3</sup> of Cr to render it semi-insulating.

The SI-MQW device was reported to show large absorption changes ( $\Delta\alpha \sim 6000$  cm<sup>-1</sup> for 20-V applied voltage) and refractive-index changes ( $\Delta n \sim 0.06$  for 20-V applied voltage) near the exciton peak at 850 nm. With only 3 mW of power incident upon the SI-MQW, a correlator based on this device showed a rise time of 1  $\mu$ s in its autocorrelation peak, an erasure time as short as 2  $\mu$ s and a controllable storage time of 2-25  $\mu$ s.

Some concerns with this type of SI-MQW are: (1) the undesirability of having Cr in a MBE system in the fabrication process, (2) large grating spacing (20-30 pm) required due to substantial charge migration at the interface. Other potential materials for fabricating these devices are Fe-doped InGaAs/InP or InGaAsP/InP and low-temperature grown Si AlGaAs/GaAs.



6. See, for example, P. Gunter and J.-P. Huignard, "Photorefractive effects and materials," in *Photorefractive Materials and Their Applications I*, ed. by P. Gunter and J.-P. Huignard, Springer-Verlag, Berlin, 1989, p.7; J. Feinberg and K. H. MacDonald, "Phase-conjugate mirrors and resonators with photorefractive materials," in *Photorefractive Materials and Their Application II*, ed. by P. Gunter and J.-P. Huignard, Springer-Verlag, 1989, p.151; T.J. Hall, "Optical information processing," in *Principles of Modern Optical Systems*, ed. by I. Andonovic and D. Ottamchandani, Artech House, Norwood, MA, 1989, p.461.
7. L.J. Cheng and A. Partovi, "Temperature and intensity dependence of photorefractive effect in GaAs," *Appl. Phys. Lett.* 49, 1456-1458 (1986).
8. G. Gheen and L.J. Cheng, "Image processing by four-wave mixing in photorefractive GaAs," *Appl. Phys. Lett.* 51, 1481-1483 (1987).
9. G. C. Valley, A. L. Smirl, M. B. Klein, K. Bohnert, and T. F. Boggess, "Picosecond photorefractive beam coupling in GaAs," *Opt. Lett.*, 11, 647-649 (1986).
10. L. J. Cheng and A. Partovi, "Index grating lifetime in photorefractive GaAs," *Appl. Opt.*, 27, 1760-1763 (1988).
11. A. M. Glass and J. Strait, "The photorefractive effect in semi conductors," in *Photorefractive Materials and Their Application I*, ed. by P. Grunter and J.P. Huignard, Springer-Verlag, Berlin, 1988, p.237.
12. R. V. Johnson and A. R. Tanguay, Jr., "Fundamental physical limitations of the photorefractive grating recording sensitivity," in *Optical Processing and Computing*, ed. by H. H. Arsenault, T. Szoplik and B. Macukow, Academic Press, New York, 1989, p.59.
13. L. J. Cheng, J. Lagowski, M. F. Rau, and F. C. Wang, "Defects and photorefractive effects in GaAs," *Radiation Effect and Defects in Solids*, 111 & 112, 37-43 (1989).
14. D. T. H. Liu, L. J. Cheng, M. F. Rau, and F. C. Wang, "Photorefractive gain in GaAs under a dc electric field," *App. Phys. Lett.*, 53, 1369-1371 (1988); D. T. H. Liu, L. J. Cheng, A. E. Chiou, and P. Yeh, "Two-beam coupling gain in undoped GaAs with applied dc electric field and moving grating," *Opt. Comm.*, 72, 384-386 (1989).
15. B. Imbert, H. Rajbenbach, S. Mallick, J. P. Herriau and J. P. Huignard, "High photorefractive gain in two-beam coupling with moving fringes in GaAs:Cr crystals," *Opt. Lett.*, 13, 327-329 (1988).
16. A. Partovi, A. Kost, E.M. Garmire, G. C. Valley and M. B. Klein, "Eland-edge photorefractive effect in semiconductors," *Appl. Phys. Lett.*, 56, 1089-1091 (1990).
17. A. Partovi, J. Millerd, and E. M. Garmire, "Large photorefractive beam-coupling gain using the Franz-Keldysh electrorefractive effect in temperature-stablized InP:Fe," *Digest of the First International Meeting on Nonlinear Optics, Kauai, Hawaii, July 16-20, 1990*, pp. 212-213.
18. D. L. Staebler and J.J. Amodei, "Coupled-wave analysis of holographic storage in LiNbO<sub>3</sub>," *J. Appl. Phys.* 43, 1042-1049 (1971).
19. N. V. Kukhtarev, B. Matkov, S. G. Odulov, M. S. Soskin and V. L. Vincitsskii, "I holographic storage in electrooptic crystals. I. Steady state," *Ferroelectrics*, 22, 949-960 (1979) and " Holographic storage in electrooptic crystals. II. Beam coupling-light amplification," 22, 961-964 (1979).

20. L. J. Cheng, G. Gheen, T. H. Chao, H. K. Liu, A. Partovi, J. Katz, and E. Garmire, "Spatial light modulation by beam coupling in GaAs crystals," *Opt. Lett.*, 12, 705-707 (1987); L. J. Cheng, G. Gheen, F. C. Wang, and M. F. Rau, "Image transfer in photorefractive GaAs," *J. Appl. Phys.*, 62, 3991-3993 (1987).
21. G. Gheen and L. J. Cheng, "Optical correlators with fast updating speed using photorefractive semiconductor materials," *Appl. Opt.*, 27, 2756-2760 (1988).
22. D. T. H. Liu, L. J. Cheng, T. H. Chao, J. W. Yu, and D. A. Gregory, "Real-time optical correlator using photorefractive GaAs," *Proc. SPIE* 1347, 156-168 (1990).
23. L. J. Cheng and D. T. H. Liu, "optical computing and image processing using photorefractive gallium arsenide," *Jap. J. Appl. Phys.*, 29, 1297-1300 (1990).
24. L. J. Cheng and D. T. H. Liu, "High-speed parallel optical processors of photorefractive semiconductors," Vol. 9 of Technical Digest of the Topical Conference on Optical Computing, Salt Lake City, Utah, February 28-March 2, 1989, p.87.
25. L. J. Cheng and D. T. H. Liu, "Properties and applications of photorefractive GaAs," *Proc. SPIE* 1220, 1-16 (1990).
26. P. Yeh, "Photorefractive two-beam coupling in cubic crystals," *J. Opt. Soc. Am. B*, 4, 1382-1386 (1987).
27. L. J. Cheng and P. Yeh, "Cross-polarization beam coupling in photorefractive GaAs crystals," *Opt. Lett.*, 13, S0-S2 (1988).
28. A. Partovi, E. Garmire, and L. J. Cheng, "Enhanced beam coupling modulation using the polarization properties of photorefractive GaAs," *Appl. Phys. Lett.* 51, 299-301 (1987).
29. M. D. Levenson, "High resolution imaging by wave-front conjugation," *Opt. Lett.* 5, 182-184 (1980).
30. A. E. Chiou and P. Yeh, "Parallel image subtraction using a phase-conjugate Michelson interferometer," *Opt. Lett.*, 11, 306-308 (1986).
31. A. E. Chiou, P. Yeh and M. Khoshnevisan, "Coherent image subtraction using phase conjugate interferometry," *Proc. SPIE* 613, 201-206 (1986).
32. S. K. Kwong, G. Rakuljic, and A. Yariv, "Real time image subtraction and 'exclusive or' operation using a self-pumped phase conjugate mirror," *Appl. Phys. Lett.*, 48, 201-203 (1986).
33. S. K. Kwong, G. Rakuljic, V. Leyva, and A. Yariv, "Real-time image processing using a self-pumped phase conjugate mirror," *Proc. W'ifi*, 613, 36-42 (1986).
34. P. Yeh, T. Y. Chang, P. H. Beckwith, "Real-time optical image subtraction using dynamic holographic interference in photorefractive media," *Opt. Lett.* 13, 586-588 (1988).
35. N. V. Vainos, J. K. Khoury, and R. W. Eason, "Real-time parallel optical logic in photorefractive bismuth silicon oxide," *Opt. Lett.*, 13, 503-505 (1988).
36. D. Z. Anderson, D. M. Lininger, and J. Feinberg, "Optical tracking novelty filter," *Opt. Lett.*, 12, 123-125 (1987).
37. D. Z. Anderson and J. Feinberg, "Optical novelty filters," *IEEE J. Quant. Electr.* QE-25, 635-637 (1989).
38. D. T. H. Liu and L. J. Cheng, "Resolution of a target-tracking optical novelty filter," *Opt. Eng.* 30, 571-576 (1991).

39. See, for example, J. Goodman, "Introduction to Fourier Optics", McGraw-Hill, New York (1968).
40. D. M. Pepper, J. Auyeung, D. Fekete, and A. Yariv, "Spatial convolution and correlation of optical fields via degenerate four wave mixing," *Opt. Lett.* 3, 7-9 (1978).
41. J. O. White and A. Yariv, "Real-time image processing via four-wave mixing in photorefractive materials," *Appl. Phys. Lett.* 37,5-7 (1980).
42. L. Pichon and J. P. Huignard, "Dynamic joint-Fourier transform correlator by Bragg diffraction in photorefractive  $\text{Bi}_{12}\text{SiO}_{20}$  crystals," *Opt. Comm.* 36,277-280 (1981).
43. P. D. Foote, T. J. Hall, and L. M. Connors, "High speed two input real-time optical correlation using photorefractive BSO," *Opt. Laser Technol.* 18, 39-42 (1986).
44. M. G. Nicholson, I. R. Cooper, M. W. McCall, and C. R. Petts, "Simple computational model of image correlation by four-wave mixing in photorefractive media," *Appl. Opt.* 26,278-286 (1987).
45. M. G. Nicholson, I. R. Cooper, G. G. Gibbons, and C. R. Petts, "Optimization of an updatable optical image correlator," *Opt. Eng.* 26, 445-452 (1987).
46. F. T. S. Yu, S. Wu, A. W. Mayers, and S. Rajan, "Wavelength-multiplexed reflection matched spatial filters," *Opt. Comm.* 81, 343-347 (1991).
47. F. T. S. Yu, S. Wu, S. Rajan, and D. A. Greg "Compact joint transform correlator with a thick photorefractive crystal," *Appl. Opt.* 31,2416-2418 (1992).
48. D. T. H. Liu and L. J. Cheng, "Real-time VanderLugt optical correlator using photorefractive GaAs," *Appl. Opt.*, 31,5675-5680 (1992).
49. A. VanderLugt, "Signal detection by complex spatial jittering," *IEEE Trans. Information Theory*, IT-10, 139-145 (1964).
50. L. J. Cheng, D. T. H. Liu and K. L. Luke, "Photorefractive image processing using compound semiconductors," *Int. J. Opt. Comp.*, in press.
51. D. T. H. Liu, T. H. Chao and L. J. Cheng, "Novelty-filtered optical correlator using photorefractive crystal" *Proc. SPIE*, 1701, 105-110 (1992),
52. L. Samuelson, "Defect levels in semiconductor alloys," *Proceedings of the 13th International Conference on Defects in Semiconductors*, ed. by L.C. Kimerling and J.M. Parsey, The Metallurgical Society of AIME, Warrendale, PA. 1984, pp. 101-114.
53. W. T. Maloney, "Acoustooptical approaches to radar signal processing," *IEEE Spectrum* 6,40-48 (1969) and references therein.
54. W. T. Rhodes, "Acousto-optic signal processing: convolution and correlation," *Proc. IEEE* 69,65-79 (1981).
55. D. Psaltis, J. Yu, and J. Hong, "Bias-free time-integrating optical correlator using a photorefractive crystal," *Appl. Opt.* 24,3860-3865 (1985).
56. J. H. Hong and T. Y. Chang, "Photorefractive time-integrating correlator," *Opt. Lett.* 16, 333-335 (1991).
57. D. T. H. Liu, K. L. Luke and L. J. Cheng, "GaAs-based photorefractive time-integrating correlator," *SPIE* 1702, 205-209 (1992).
58. D. T. H. Liu, K. L. Luke and L. J. Cheng, unpublished results.
59. A. Partovi, A. M. Glass, T. H. Chiu and D. T. H. Liu, "High-speed joint-transform optical image correlator using GaAs/AlGaAs semi-insulating multiple quantum wells and diode lasers," *Opt. Lett.* 18,906-908 (1993).